PNAS

Supporting Information for
SMARCB1 regulates the hypoxic stress response in sickle cell trait.

Melinda Soeung[1,*], Luigi Perelli[2,†], Ziheng Chen[1,†], Eleonora Dondossola[2,3], I-Lin Ho[1], Federica Carbone[4], Li Zhang[2], Hania Khan[2], Courtney N. Le[2], Cihui Zhu[2], Michael D. Peoples[5], Ningping Feng[5], Shan Jiang[5], Niki Millward Zacharias[6], Rosalba Minelli[5], Daniel D. Shapiro[7], Angela K. Deem[1], Sisi Gao[1], Emily H. Cheng[8], Donatella Lucchetti[9,10], Cheryl L. Walker[11], Alessandro Carugo[5,12], Virginia Giuliani[5], Timothy P. Heffernan[5], Andrea Viale[1], Nizar M. Tannir[2], Giulio F. Draetta[1,5], Pavlos Msaouel[2,3,11,13,#,*], Giannicola Genovese[1,2,3,5,#,*]

[1]Department of Genomic Medicine, The University of Texas MD Anderson Cancer Center, Houston, USA
[2]Department of Genitourinary Medical Oncology, The University of Texas MD Anderson Cancer Center, Houston, USA
[3]David H. Koch Center for Applied Research of Genitourinary Cancers, The University of Texas, MD Anderson Cancer Center, Houston, USA
[4]Nerviano Medical Sciences, NMS Group Spa, 20014, Nerviano, Milan, Italy
[5]Translational Research to Advance Therapeutics and Innovation in Oncology (TRACTION), The University of Texas MD Anderson Cancer Center, Houston, TX, USA
[6]Department of Urology, The University of Texas MD Anderson Cancer Center, Houston, TX, USA.
[7]Division of Urology, William S. Middleton Memorial VA Hospital, Madison, USA
[8]Human Oncology & Pathogenesis Program and Department of Pathology, Memorial Sloan Kettering Cancer Institute, New York City, NY 10065, USA
[9]Department of Translational Medicine and Surgery - Faculty of Medicine and Surgery, Catholic University of the Sacred Heart Rome, Italy
[10]Fondazione Policlinico Universitario "A. Gemelli" - IRCCS, Rome, Italy
[11]Center for Precision Environmental Health, Baylor college of Medicine, Houston, Texas, USA
[12]Department of Oncology, IRBM S.p.A., Via Pontina Km 30 600, Pomezia, Rome 00071, Italy
[13]Department of Translational Molecular Pathology, The University of Texas MD Anderson Cancer Center, Houston, USA

†L.P. and Z.C. contributed equally to this work.
#G.G. and P.M. contributed equally to this work.
*Corresponding authors: GGenovese@mdanderson.org; PMsaouel@mdanderson.org; MSoeung@mdanderson.org

Dr. Giannicola Genovese, M.D., Ph.D.
E-mail: GGenovese@mdanderson.org

Dr. Pavlos Msaouel, M.D., Ph.D.
E-mail: PMsaouel@mdanderson.org

Dr. Melinda Soeung, Ph.D.
E-mail: MSoeung@mdanderson.org

This PDF file includes:

Supporting methods
SI Figures S1 to S4
Table S1
SI Appendix References

Supporting Methods

In vivo studies

Genotyping conditions:

Townes model (hα/hα::β^A/β^S): The common (mouse beta KI) forward primer is 5'- TTGAGCAATGTG GACAGAGAAGG; the Beta A reverse primer is 5'- GTTTAGCCAGGGACCGTTTCAG; the Beta S reverse primer is 5'- AATTCTGGCTTATCGGAGGCAAG; the reverse primer for mouse beta wild type is 5'- ATGTCAGAAGCAAATGTGAGGAGCA. The separated PCR conditions are as follows: 94°C for 2 minutes, continue PCR for 10 cycles at 94°C for 20 seconds, 65°C with 0.5°C decrease per cycle for 15 seconds, 68°C for 10 seconds, continue PCR for 28 cycles at 94°C for 15 seconds, 60°C for 15 seconds, 72°C for 10 seconds.

Cdh16-Cre: The forward primer for the transgene is 5'- GCAGATCTGGCTCTCCAAAG; the forward primer for the internal positive control is 5'- CAAATGTTGCTTGTCTGGTG; the reverse primer for the internal positive control is 5'- GTCAGTCGAGTGCACAGTTT; the reverse primer for the transgene is 5'- AGGCAAATTTTGGTGTACGG. The touchdown PCR cycling conditions are as follows: 94°C for 2 minutes, continue PCR for 10 cycles at 94°C for 20 seconds, 65°C with 0.5°C decrease per cycle for 15 seconds, 68°C for 10 seconds, continue PCR for 28 cycles at 94°C for 15 seconds, 60°C for 15 seconds, 72°C for 10 seconds.

Rosa26$^{LSL\text{-}TdT}$ allele: The forward primer for wild-type Tomato is 5'- AAGGGAGCTGCAGTGGAGTA; the reverse primer for wild-type Tomato is 5'- CCGAAAAATCTGTGGGAAGTC; the forward primer for Tomato mutant is 5'- CTGTTCCTGTACGGCATGG; the reverse primer for Tomato mutant is 5'- GGCATTAAAGCAGCGTATC. The touchdown PCR cycling conditions are as follows: 10 cycles at 94°C for 20 seconds, 65°C and 0.5°C per cycle decrease for 15 seconds,

68°C for 10 seconds. Continue the PCR reaction for 28 cycles at 94°C for 15 seconds, 60°C for 15 seconds, 72°C for 10 seconds.

Rosa26-Cas9 knockin on C57BL/6J allele: The forward primer for wild-type is 5'- CTGGCTTCTGAGGACCG; the reverse primer for wild-type is 5'- AGCCTGCCCAGAAGACTCC. The forward primer for mutant is 5'- GCTAACCATGTTCATGCCTTC; the reverse primer for mutant is 5'- CTCCGTCGTGGTCCTTATAGT. The touchdown PCR cycling conditions are as follows: 10 cycles at 94°C for 20 seconds, 65°C and 0.5°C per cycle decrease for 15 seconds, 68°C for 10 seconds. Continue the PCR reaction for 28 cycles at 94°C for 15 seconds, 60°C for 15 seconds, 72°C for 10 seconds.

Ex vivo multiphoton microscopy analysis of mouse models:

To measure renal ischemia using ex vivo multiphoton microscopy analysis(*1*), four adult wild-type mice and five SCT mice were injected with fluorescein isothiocyanate (FITC)–dextran 500,000 KDa (Sigma Aldrich) and euthanized after five minutes followed by kidney removal for multiphoton microscopy analysis of perfusion of the renal medullary vasculature. The large molecular weight dextran was used to prevent filtration outside the renal tubules. Kidneys were removed and monitored by multiphoton microscopy (Trimscope II, LaVision BioTech) using a long working distance 25x NA 1.05 oil/water objective (Olympus). The microscope was equipped with three titanium (Ti):sapphire lasers (Chameleon-XR, Coherent) and two optical parametric oscillators (APE/Coherent), resulting in a tunable excitation range from 800 to 1300 nm. Detection of blood vessels and kidney cells was achieved by spectral separation of FITC (525/50, 920 nm) and RFP (595/40, 1090 nm), and 3D stacks were obtained for up to 300 µm depth at 10 µm step size. Images from individual 3D stacks were reconstructed and analyzed using FIJI. Vessel diameter and length were measured manually. The diameter was measured in 10 vessels/image, in three different location within each vessel. The length was measured in 10 vessels/image.

Pimonidazole hydrochloride (Hypoxyprobe):

Renal hypoxia was measured using pimonidazole hydrochloride (Hypoxyprobe). Adult wild-type mice (n=52) and mice with SCT (n=31) were injected with 100 µL of 60 mg/kg of pimonidazole hydrochloride three hours prior to sacrifice. Mice were then anesthetized using isoflurane (Henry Schein Animal Health), and kidneys were removed and immediately fixed with 10% formalin for 24 hours at room temperature for further IHC studies. The amount of time between removal of the kidneys from mice and fixing in formalin was minimized in order to accurately measure tissue hypoxia.

In vivo treatment study in NOD scid gamma (NSG) mice

NSG female mice were subcutaneously injected with $1x10^6$ RMC219-tet-inducible and RMC219-tet-empty cells resuspended in 200 µL of 1:1 Matrigel (BD Biosciences, 356231) and media mixture. Cells were cultured off doxycycline prior to transplantation. Once the tumor reached approximately $100mm^3$ mice were placed on doxycycline water for three days before starting treatment with axitinib (Selleckchem, # AG 013736). Mice were kept on doxycycline water throughout the experiment. Doxycycline water was supplemented with sucrose to encourage mice to drink the doxycycline water. Regular water was removed throughout the experiment. Axitinib was administered via oral gavage at 30mg/kg every day for 14 days (n=10). Axitinib was dissolved in 0.5% CMC solution. Control mice received 0.5% CMC vehicle alone (n=10). Tumor volume was measured every three days by caliper, and the body weight was also monitored. Tumor volume (mm^3) was calculated using the following formula: V (mm^3) = L (mm) × W (mm) 2 /2, where W is tumor width and L is tumor length. Mice were sacrificed after 14 days of treatment according to approved guidelines of the Institutions Animal Ethics Committee. Tumors were harvested, weighed, and fixed in formalin for histological analysis.

Immunohistochemistry (IHC)

IHC was performed on FFPE whole kidney sagittal sections. The sagittal kidney sections were fixed in 10% formalin, embedded, and 5 µm sections were cut using a microtome (Leica RM2235). The sections were then baked on slides, de-paraffinized, and treated with citrate

buffer (Electron Microscopy Sciences) for antigen retrieval according to the manufacturer's instructions. Endogenous peroxidases were then inactivated using 3% hydrogen peroxide (Sigma-Aldrich) for 10 minutes followed by washing with phosphate buffer saline. Non-specific signals were then blocked for 20 minutes using Rodent Block M (Biocare Medical). Samples were then stained with 1:200 primary Hypoxyprobe (Hypoxyprobe, #2627) antibody conjugated with horseradish peroxidase (HRP) for 12 hours overnight in 4°C. After an overnight incubation, slides were washed three times using phosphate buffer saline before staining with Rabbit-on-Rodent HRP polymer (Biocare Medical) for one hour at room temperature. NovaRED peroxidase substrate (Vector Lab, #SK-4800) or 3,3'-Diaminobenzidine (DAB) was used for HRP detection (10 minutes of exposure). Hematoxylin was used for counterstaining and eosin was used to detect the cytoplasm of cells in tissue slides. A Nikon EclipseTi microscope and Nikon DS-Fi1 digital camera were used to capture 20x images. The following antibodies were used for IHC analysis: anti-CD31 (PECAM-1, D8V9E) (Cell Signaling Technology, #77699, 1:100 dilution), anti-SMARCB1 (Sigma Aldrich, #HPA018248, 1:100), and eIF2-alpha (EIF2S1, Invitrogen, #AHO0802).

Equal areas of each 20x image were then quantified using ImageJ/FIJI. Using FIJI, the IHC images were deconvoluted into three channels. The optical densities of the DAB channel images were then quantified and graphed into GraphPad for further statistical analysis. During the quantification of IHC, the genotypes of the mice were blinded to the experimenter to minimize bias, and only the mice toe numbers was known to the experimenter. Genotypes were included in the final graphs for the final manuscript.

Single-guide RNA design and validation

Single-guide RNAs (sgRNAs) were designed with "GenScript CRISPR sgRNA Design Tool". First, 5`-phosphorilated oligos were annealed and diluted 1:20. Then 1 uL of each annealed and diluted sgRNA was cloned in digested lentiCRISPR V2 (addgene #52961) according to Dr. Feng Zhang's protocol. NEB® Stable Competent *E. coli* (C3040I) colonies resistant to ampicillin antibiotic selection were amplified, and

presence of sgRNA was confirmed by Sanger sequencing. Positive clones were transfected individually in 293 cells along with vectors for lentiviral packaging production, PAX2 (addgene #12260) and PMD2G (addgene #12259). MCT cells were infected by the lentivirus carrying a specific sgRNA and selected for puromycin resistance. Cut efficiency of sgRNA was tested by T7 Endonuclease I (NEB #M0302L) assay on the DNA of infected cells, according to the protocol. Single-guide RNA-mediated deletion was tested by PCR amplification.

sgRNA sequences:

sgSMARCB1-exon1

GCTTGACGGGCTTCTGCCCGA

sgSMARCB1-exon2

GAGAACCTCGGAACATACGC

sgTRP53

GACACTCGGAGGGCTTCACT

sgCDKN2A

GTGCGATATTTGCGTTCCGC

sgCDKN2B

GGCGCCTCCCGAAGCGGTTC

Surgical procedures

Orthotopic injection in kidney.

First, 10^{10} adeno-associated viral particles were resuspended in PBS (Thermo Fisher Scientific) and Matrigel matrix (Corning) 1:1 solution. Six- to nine-week-old mice were shaved and anesthetized using isoflurane (Henry Schein Animal Health). Analgesia was achieved with buprenorphine SR (0.1 mg/Kg BID) (Par Parmaceutical) via subcutaneous injection, and shaved skin was disinfected with 70% ethanol and betadine (Dynarex). A 1-cm incision was performed on the left flank through the skin/subcutaneous and muscular/peritoneal

layers. Left kidney was exposed and 20 uL of viral resuspension was introduced by Hamilton syringe into the organ by a subcapsular injection. Hemostasis was controlled with a bipolar cautery (Bioseb) if needed. The kidney was carefully repositioned into the abdominal cavity, and muscular/peritoneal planes were closed individually by absorbable sutures. The skin/subcutaneous planes were closed using metal clips. Mice were monitored daily for the first three days, and twice/week thereafter for signs of tumor growth by manual palpation.

Euthanasia, necropsy, and tissues collection

Mice were euthanized by exposure to CO_2 followed by cervical dislocation. A necropsy form was filled in with mouse information, tumor size and weight, infiltrated organ annotations, and metastasis number and location.

Tumor cell isolation and culture

Ex vivo cultures from primary tumor explants were generated by mechanical dissociation and incubation for 1 hour at 37°C with a solution of collagenase IV/dispase (4 mg/mL) (Invitrogen), resuspended in DMEM (Lonza) and filtered. Cells derived from tumor dissociation and digestion were plated on gelatin 0.1% (Millipore Sigma) coated plates and cultured in DMEM (Lonza) supplemented with 20% FBS (Lonza) and 1% penicillin–streptomycin and kept in culture for less than 5 passages.

MRI Imaging:

This procedure has been described in previous studies. A 7T Bruker Biospec (BrukerBioSpin), equipped with 35 mm inner diameter volume coil and 6 cm inner-diameter gradients, was used for imaging the animals. A fast acquisition with relaxation enhancement (RARE) sequence with TR/TE of 2,000/38 ms, matrix size 256× 192, 0.75 mm slice thickness, 0.25 mm slice gap, 4× 3 cm FOV, 101 kHz bandwidth, 3 NEX was used for acquired in coronal and axial geometries a multi-

slice T2-weighted images. To reduce the respiratory motion the axial scan sequences were gated.

In vitro studies

Cell lines

mIMCD-3(*2*) cells were cultured in Dulbecco's modified Eagle's medium (DMEM/F12) (ThermoFiscer Scientific) supplemented with 1% pencillin-streptomycin (Gibco) and 10% fetal bovine serum (FBS) (Gibco). MCT (mouse cortical tubules)(*3*) cells were cultured in Dulbecco's modified Eagle's medium (DMEM) (ThermoFiscer Scientific) supplemented with 1% pencillin-streptomycin (Gibco) and 10% fetal bovine serum (FBS) (Gibco). Cell lines were cultured in at 37^{o}C with 5% CO_2. All cells were tested for Mycoplasma contamination using ABM PCR mycoplasma detection kit, catalog#G238.

MSRT1 cells were generated in our lab using CRISPR Cas9 gene editing technology. We injected orthotopically a guide package containing sg*SMARCB1,* sg*TP53* into the right kidneys sub-capsular of C57BL/6J pure background mice with Rosa26-Cas9-GFP (from Feng Zhang lab, to add in the methods if it's not there) knockin. The Rosa26-Cas9-GFP knockin mice have constitutively active Cas9 with a GFP reporter. Twelve mice were injected, and 33% of mice developed aggressive kidney tumors within two months. Histological evaluation of renal tumors showed rhabdoid-like features that are characteristic of *SMARCB1* knockout (**SI Appendix**, **Fig. S1**). MSRT1 tumor cell line was then established from tumors and used for further *ex vivo* studies. Immunoblotting analysis of renal tumor cell line confirmed that cell lines were negative for SMARCB1 protein (**SI Appendix**, **Fig. S1**). We performed whole exome sequencing (WES) analysis on the MSRT1 cell line in comparison to corresponding normal mouse kidney cells. Using Integrative Genomics Viewer (IGV), our WES analysis showed that there is efficient sgRNA-targeted cutting of *smarcb1* (exons 1 and 2) and *cdkn2a/b* (**SI Appendix**, **Fig. S4**). WES analysis also indicates that sgRNA for *trp53* did not result in CRISPR/Cas9 cutting of *trp53* (**SI Appendix**, **Fig. S4e**), but there is a spontaneous focal alteration at both exon 3 and 4 (**SI Appendix**, **Fig.**

S4f), explaining why we see the loss of TP53 protein in immunoblotting analysis after subjecting cells to ten seconds of exposure to ultraviolet light to induce the expression of TP53 (**SI Appendix**, **Fig. S1h**).

Immunoblotting/Western Blotting:

Cells were lysed with RIPA buffer containing protease inhibitor. Protein lysates were resolved on 5–15% gradient polyacrylamide SDS gels and transferred onto PVDF membranes according to manufacturer's instructions. Membranes were incubated with indicated primary antibodies, washed in TBST buffer and probed with HRP-conjugated secondary antibodies. The detection of bands was carried out upon chemiluminescence reaction followed by film exposure. The following antibodies were used: anti-SMARCB1 (Sigma Aldrich, #HPA018248, 1:200 dilution), anti-VINCULIN (Cell Signaling Technology, #4650S, 1:2000 dilution), anti- β-ACTIN (Cell Signaling Technology, #4967S, 1:2000 dilution), and HIF-1α (D2U3T) (Cell Signaling Technology, #14179, 1:1000). The following reagents were used for measuring protein stability: MG-132 (Selleckchem, #S2619) and cycloheximide (Selleckchem, #NSC-185). Compounds were diluted in Dimethyl sulfoxide (DMSO) (Sigma Aldrich, #67-68-5), and DMSO equivalent was used as the vehicle.

Immunoprecipitation (IP):

For IP experiments, cell lysates were prepared using RIPA buffer containing protease inhibitor. 5 µg of anti-SMARCB1 (Bethyl laboratories, #A301-087A) was incubated with 50 µL of Protein A Magnetic Beads (New England BioLabs, #S1425S) overnight at 4C. Afterwards, beads were washed three times with phosphate buffer saline (PBS), and incubated with 1 mg of protein lysate overnight at 4^{o}C. After overnight incubation, beads were washed with PBS eight times in 4^{o}C. To elute beads, beads were incubated with 0.1 M glycine at room temperature for 10 minutes. Elution was then removed from beads (careful not to include beads) and used for further immunoblotting analysis. To avoid detection of heavy chain, anti-SMARCB1 (BD laboratories, #612110) was used for immunoblotting

analysis. Anti-UBIQUITIN (P4D1) antibody (Cell Signaling Technology, #3936, 1: 1000) was used to measure ubiquitination after IP.

We selected six hours of hypoxia for the IP analyses because exposing cells to hypoxia for greater than six hours results in the strong degradation of SMARCB1 protein. This would thus impair our ability to isolate enough protein for the IP analysis.

Site-directed mutagenesis (SDM).

The amino acid sequence for SMARCB1 (human) was retrieved from NCBI (source: https://www.ncbi.nlm.nih.gov/projects/CCDS/CcdsBrowse.cgi?REQUEST=GV&DATA=574903&BUILDS=CURRENTBUILDS). Listed lysine (K) and arginine (R) residues (See Table 1) were converted to arginine (R) and histidine (H), respectively. For deletions, the residue was replaced by a STOP codon. Hotspot mutations R377H, K364, and K363 deletion were also included in this study. SMARCB1 mutant sequences and wild-type sequence were then cloned into pDONR 221 Gateway donor vector (Invitrogen). Gateway cloning method was used to ligate donor vector into destination vector pHAGE-IRES-PURO. SMARCB1 mutants were then reconstituted into SMARCB1 deficient cell lines, and positive clones were selected using puromycin.

Virus preparation:

Infectious viral particles were produced using helper plasmids psPAX2 and pMD2G obtained through Addgene. 293T cells were cultured in DMEM containing 10% FBS (Gibco), 100 µg/ml Penicillin/Streptomycin (Gibco) and transfected using the Polyethylenimine (PEI) method. Virus-containing supernatant was collected 72 hours after transfection, spun at 3000 rpm for 10 minutes and decanted (*4*). High-titer preps were obtained by a single round of ultracentrifugation at 24,000 RPM for 2.5 hours.

Clonogenic assay:

After allowing cells to grow at certain conditions, media was removed, cells were washed once with phosphate buffer saline (PBS), and 0.5% crystal violet (CV) solution was added to cells. Cells were gently incubated on a shaker at room temperature for one hour. After one hour of incubation, CV solution was removed, and residual CV was washed completely away with water. 10% acetic acid was used to dissolve CV, followed by further quantification by measuring the absorbance of CV at 550 nm using a spectrophotometer.

Flow cytometry analysis:

Collect tumors that approximately 1X1 cm in size in phosphate buffer saline (PBS, Thermofischer Scientific) supplemented with 1% pencillin-streptomycin (Gibco). Dissociate the tumor tissue using a blade until there are no large pieces present. Incubate the dissociated tumor in 10 mL of DMEM (Lonza) supplemented with 2 mg/mL collagenase and 2 mg/mL dispase for one hour at 37^{o}C. Pipette the mixture every 20 minutes. Afterwards, centrifuge the sample at 1200 rpm for five minutes, and remove supernatant. Next, resuspend the cell pellet in 2-3 mL of PBS supplemented with 5% fetal bovine serum (FBS), and filter through a 100 µm filter. After the first filter, filter again through a 40 µm filter. Filter one last time into a cytofluorimeter tube for flow cytometry (FACS) analysis.

CellTiter-Glo® 2.0 Assay (viability assay)

Cell viability was measured using CellTiter-Glo® 2.0 Assay (Promega), and manufacturer's instructions were followed. Prepare opaque-walled 96 multiwell plates with cells in 100µl of culture medium. At the timepoints of interest, equilibrate the plate and its contents to room temperature for approximately 30 minutes. After incubation, add 100 µL of CellTiter-Glo® 2.0 reagent to 100µl of medium containing cells. Do not change media before performing assay as this can change the results. Mix the contents for 2 minutes on an orbital shaker to induce cell lysis. Afterwards, allow the plate to incubate at room temperature for 10 minutes to stabilize the luminescent signal, and record luminescence using fluorimeter microplate reader.

Senescence β-Galactosidase Staining:

Senescence β-Galactosidase Staining Kit (Cell Signaling Technology, catalog# 9860) was used to measure senescent cells, and the manufacturer's protocol was followed for experiment. Cells were incubated for 24 hours with β-galactosidase at 37^{o}C before quantifying staining.

Analysis

Statistical analysis

Data was graphed using Prism GraphPad. One-way ANOVA and Tukey multiple comparison tests were used to compare the changes in β-galactosidase and cellular viability. Student's t-test was used to calculate P-value for all other analysis.

Whole exoneme sequencing data analysis:

Sequencing fasta files were applied to FastQC (*5*) for quality control, adapters were trimmed by trimmomatic (*6*), and the genomic fragments were aligned to mm10 using bwa mem (*7*), then sorted and indexed by samtools (*8*). Following Base Quality Score Recalibration (BQSR) by GATK(*9*). Somatic mutations were called by Mutect2 (*9*) and structural variants were called by Manta Structural Variant Caller (*10*).

SI Appendix figures and figure legends

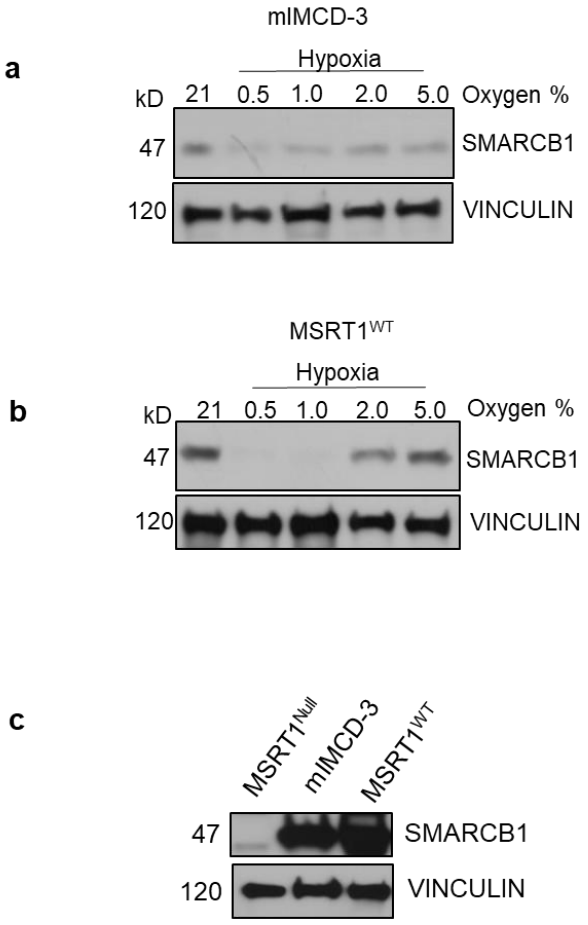

Fig. S1. SMARCB1 degradation at different oxygen percentages. mIMCD-3 **(a)** and MSRT1^{WT} **(b)** were exposed to different oxygen levels for 24 hours followed by immunoblotting analysis of SMARCB1 and VINCULIN was used as an internal control. **(c)** Ectopic overexpression of SMARCB1 in MSRT1 cell lines is equivalent to endogenous SMARCB1 in mIMCD-3 cells. Protein analysis of SMARCB1 protein levels in parental MSRT1 (MSRT1^{Null}), normal mouse kidney epithelial cells (mIMCD-3), and MSRT1 cells with ectopic overexpression of wild-type SMARCB1 (SMARCB1^{WT}).

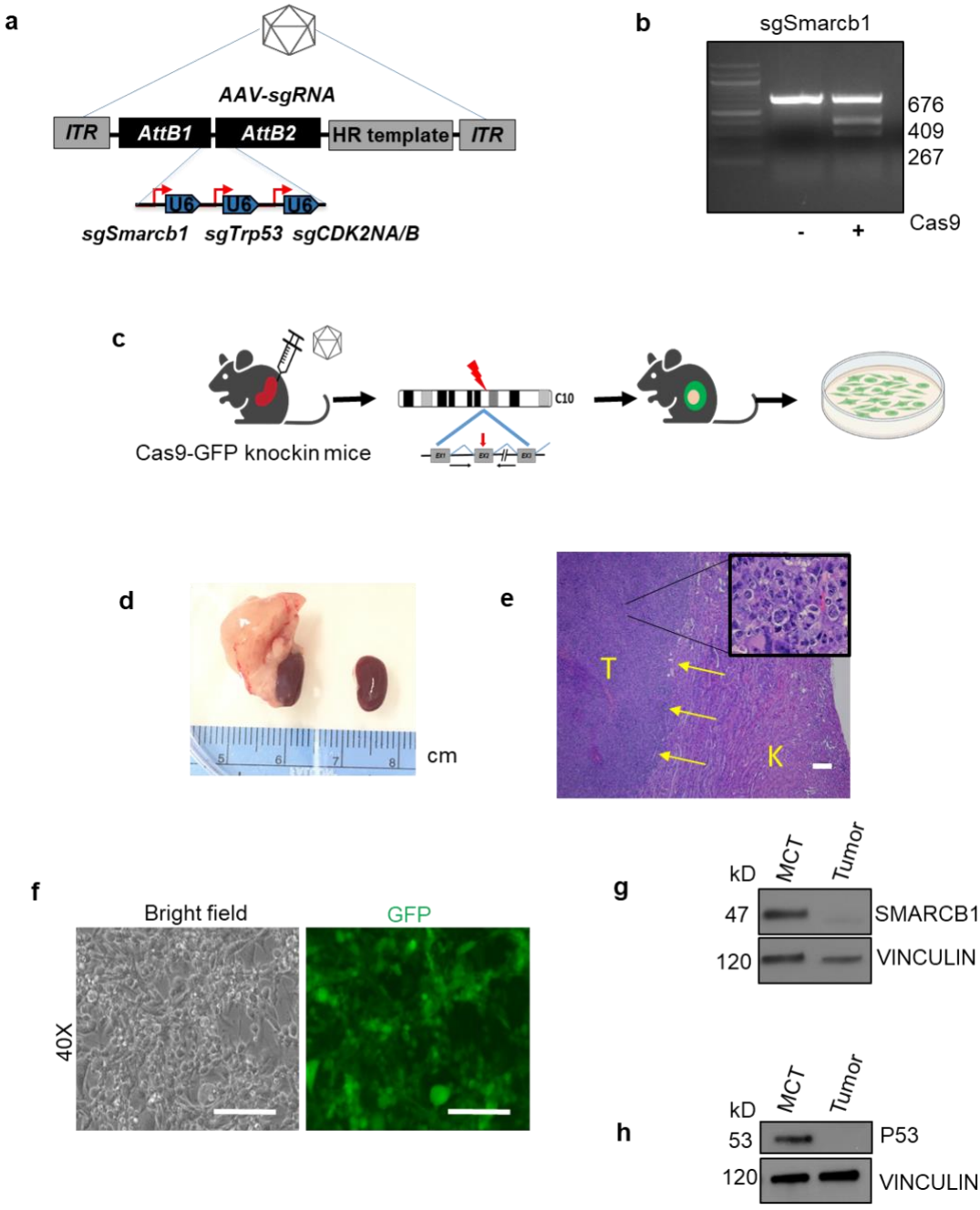

Fig. S2. Establishment of SMARCB1-deficient mouse renal tumor cell line (referred to as MSRT1). (a) Schematic of sgRNA package design. **(b)** T7 endonuclease assay demonstrating cutting efficiency of sgSMARCB1. **(c)** Schematic of workflow to generate MSRT1 cancer cell line. **(d)** Gross image of kidney tumor that developed in the left kidney of mice after introducing sgRNA package. **(e)** Histological evaluation of renal tumor cell lines generated from sgRNA for *Smarcb1*, *CDK2NA/B*, and *Trp53* injected into left kidneys

of C57BL/6J mice with Rosa26-Cas9 knockin. Yellow arrows indicate boundary between tumor (T) and renal inner medulla (K), showing that the tumor tissue arose from the inner medulla of the mouse kidney. Tumor tissue was stained with hematoxylin and eosin. **(f)** Microscopic images of tumor cell lines prepared from spontaneous tumors generated from somatic mouse model. **(g-h)** Immunoblotting of tumor cell lines derived from somatic mouse models showing successful SMARCB1 and TP53 knockout compared to normal MCT cell line that was used as a positive control.

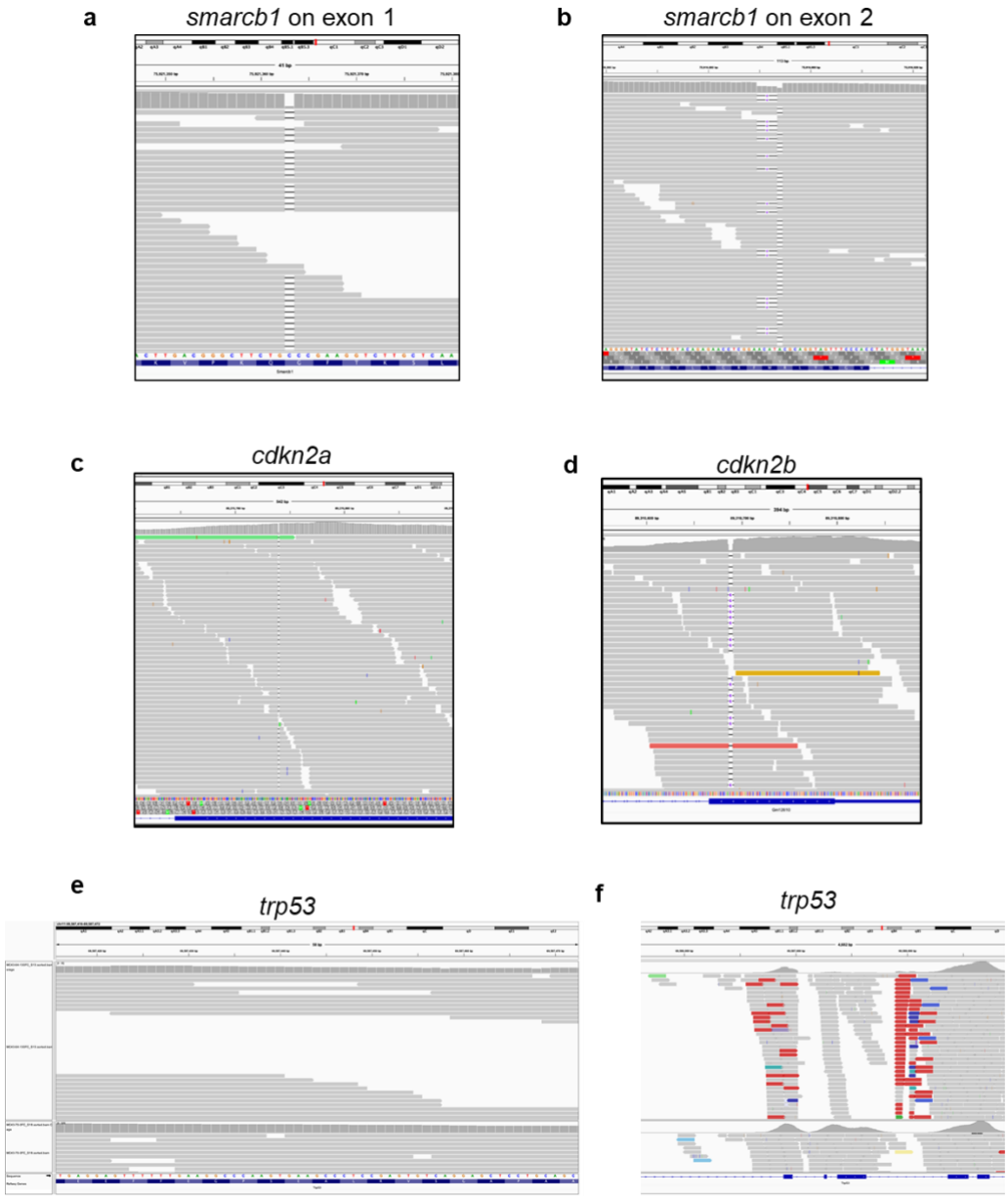

Fig. S3. Whole exome sequencing (WES) analysis of MSRT1 parental cell line. WES analysis showed efficient sgRNA-targeted cutting of **(a)** *smarcb1* on exon 1, **(b)** *smarcb1* on exon 2, **(c)** *cdkn2a*, and **(d)** *cdkn2b*. According to WES analysis, sgRNA for *trp53* did have efficient sgRNA-targeted cutting at exon 3 as expected **(e)**, but there is a spontaneous focal alteration at both exon 3 and 4 **(f)**.

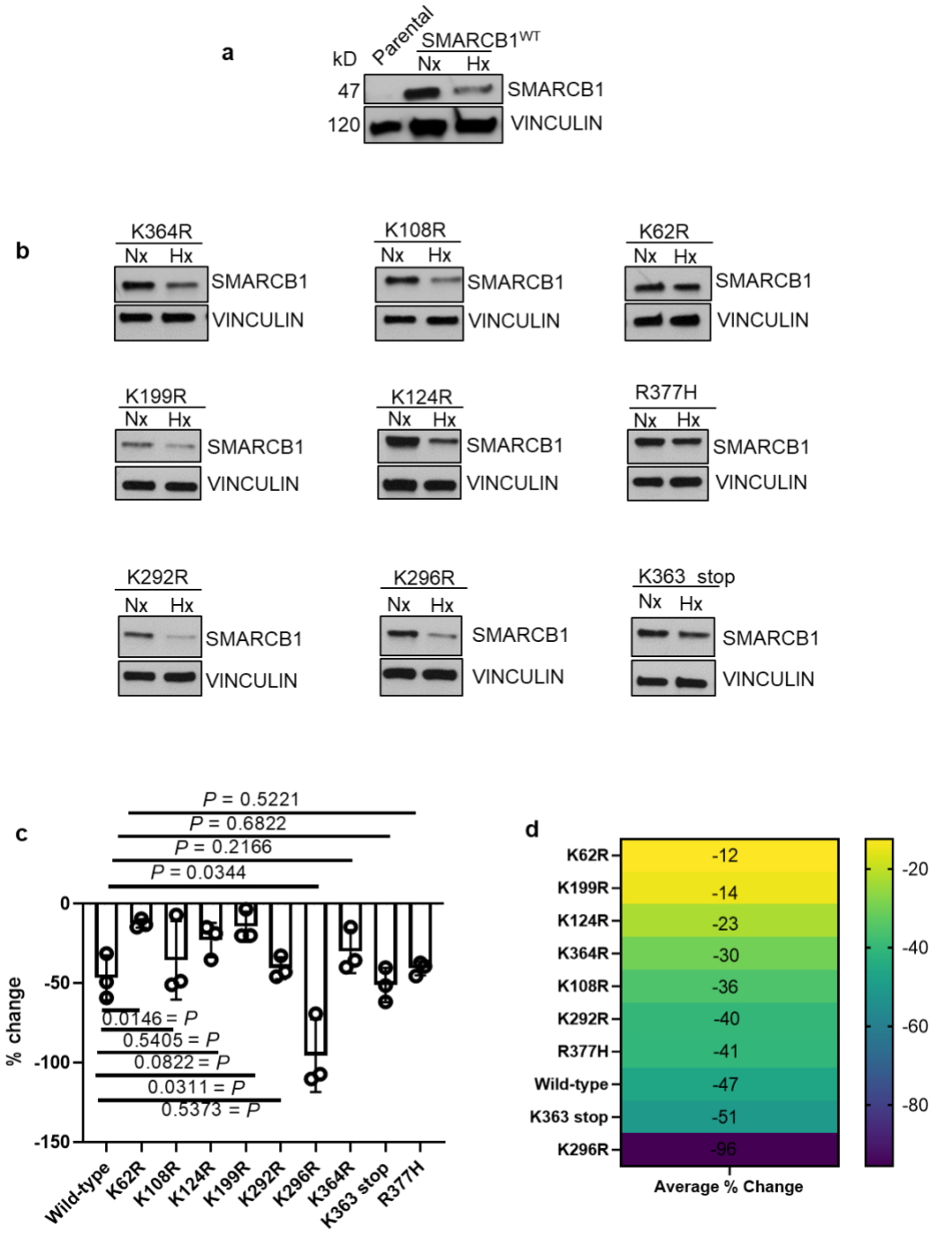

Fig. S4. Site-directed mutagenesis protein analysis showing the effects of known and new lysine residue mutations on SMARCB1 degradation. K62R has the most significant effect on preventing SMARCB1 degradation. (**a-b**) Immunoblotting of

SMARCB1 protein expression after treatment with 48 hours of hypoxia (1% oxygen) in re-constituted SMARCB1^{WT} and SMARCB1 lysine mutants. (**c**) SMARCB1 protein band was normalized to corresponding VINCULIN protein band using ImageJ FIJI software. The percent change of SMARCB1 protein levels at normoxia were compared to protein levels at hypoxia and graphed using a bar plot. Data are expressed as mean value ± SD, with *P* value calculated by student's *t* test. (**d**) Heatmap of the average percentage change of SMARCB1 protein after 48 hours of hypoxia compared to 48 hours of normoxia.

Table S1. List of residues that were mutated using site-directed mutagenesis (SDM).

Location	Modification	Residue	Reference(s)
13	Ubiquitination	K	(12) (13) (41)
62		K	
108	Ubiquitination	K	(12) (15)
124	Ubiquitination	K	(12)
199	Ubiquitination	K	(12) (16)
286	Ubiquitination	K	(17)
292	Ubiquitination	K	(12) (18) (17) (19)
296	Ubiquitination	K	(17)
363	Ubiquitination	K	(20)
364	Missense mutation	K	(42)
377	Missense mutation	R	(42)

SI Appendix References

1. E. Dondossola *et al.*, Examination of the foreign body response to biomaterials by nonlinear intravital microscopy. *Nature Biomedical Engineering* **1**, 0007 (2016).
2. M. I. Rauchman, S. K. Nigam, E. Delpire, S. R. Gullans, An osmotically tolerant inner medullary collecting duct cell line from an SV40 transgenic mouse. *The American journal of physiology* **265**, F416-424 (1993).
3. T. P. Haverty *et al.*, Characterization of a Renal Tubular Epithelial Cell Line Which Secretes the Autologous Target Antigen of Autoimmune Experimental Interstitial Nephritis. *The Journal of Cell Biology* **107**, 1359-1368 (1988).
4. G. Genovese *et al.*, microRNA regulatory network inference identifies miR-34a as a novel regulator of TGF-beta signaling in glioblastoma. *Cancer discovery* **2**, 736-749 (2012).
5. S. Andrews, FastQC: A Quality Control Tool for High Throughput Sequence Data *Babraham Bioinformatics*, (2010).
6. A. M. Bolger, M. Lohse, B. Usadel, Trimmomatic: a flexible trimmer for Illumina sequence data. *Bioinformatics* **30**, 2114-2120 (2014).
7. H. Li, R. Durbin, Fast and accurate short read alignment with Burrows–Wheeler transform. *Bioinformatics* **25**, 1754-1760 (2009).
8. H. Li *et al.*, The Sequence Alignment/Map format and SAMtools. *Bioinformatics* **25**, 2078-2079 (2009).
9. G. V. d. A. a. B. O'Connor, Genomics in the Cloud: Using Docker, GATK, and WDL in Terra (1st Edition). (2020).
10. X. Chen *et al.*, Manta: rapid detection of structural variants and indels for germline and cancer sequencing applications. *Bioinformatics* **32**, 1220-1222 (2016).
11. V. Akimov *et al.*, UbiSite approach for comprehensive mapping of lysine and N-terminal ubiquitination sites. *Nature Structural & Molecular Biology* **25**, 631-640 (2018).
12. C. M. Rose *et al.*, Highly Multiplexed Quantitative Mass Spectrometry Analysis of Ubiquitylomes. *Cell systems* **3**, 395-403.e394 (2016).
13. A. Stukalov *et al.*, Multilevel proteomics reveals host perturbations by SARS-CoV-2 and SARS-CoV. *Nature*, (2021).

14. S. A. Sarraf *et al.*, Landscape of the PARKIN-dependent ubiquitylome in response to mitochondrial depolarization. *Nature* **496**, 372-376 (2013).
15. E. Stes *et al.*, A COFRADIC protocol to study protein ubiquitination. *Journal of proteome research* **13**, 3107-3113 (2014).
16. L. K. Povlsen *et al.*, Systems-wide analysis of ubiquitylation dynamics reveals a key role for PAF15 ubiquitylation in DNA-damage bypass. *Nature cell biology* **14**, 1089-1098 (2012).
17. W. Li *et al.*, Integrative Analysis of Proteome and Ubiquitylome Reveals Unique Features of Lysosomal and Endocytic Pathways in Gefitinib-Resistant Non-Small Cell Lung Cancer Cells. *Proteomics* **18**, e1700388 (2018).
18. S. A. Wagner *et al.*, A proteome-wide, quantitative survey of in vivo ubiquitylation sites reveals widespread regulatory roles. *Molecular & cellular proteomics : MCP* **10**, M111.013284 (2011).
19. N. D. Udeshi *et al.*, Methods for quantification of in vivo changes in protein ubiquitination following proteasome and deubiquitinase inhibition. *Molecular & cellular proteomics : MCP* **11**, 148-159 (2012).
20. A. Zehir *et al.*, Mutational landscape of metastatic cancer revealed from prospective clinical sequencing of 10,000 patients. *Nature medicine* **23**, 703-713 (2017).